doi:10.1093/plphys/kiab074 PLANT PHYSIOLOGY 2021: 186: 599–610

Plant Physiology®

Research Article

The mitochondrial AAA protease FTSH3 regulates Complex I abundance by promoting its disassembly

Aneta Ivanova [1,2], Abi S. Ghifari [1,2], Oliver Berkowitz [3], James Whelan [3] and Monika W. Murcha [1,2,*,†]

1 School of Molecular Sciences, The University of Western Australia, 35 Stirling Highway, Crawley, Perth 6009, Australia
2 The ARC Centre of Excellence in Plant Energy Biology, The University of Western Australia, 35 Stirling Highway, Crawley, Perth 6009, Australia
3 Department of Animal, Plant and Soil Science, School of Life Science, The ARC Centre of Excellence in Plant Energy Biology, La Trobe University, Bundoora 3086, Vic, Australia

*Author for communication: monika.murcha@uwa.edu.au.
†Senior author.

A.I., J.W., and M.W.M. designed the research; A.I., A.S.G., O.B., and M.W.M. performed the research; all authors analyzed the data and contributed to writing the paper.
The author responsible for distribution of materials integral to the findings presented in this article in accordance with the policy described in the Instructions for Authors (https://academic.oup.com/plphys/pages/general-instructions) is: Monika W. Murcha (monika.murcha@uwa.edu.au).

Abstract

ATP is generated in mitochondria by oxidative phosphorylation. Complex I (NADH:ubiquinone oxidoreductase or NADH dehydrogenase) is the first multisubunit protein complex of this pathway, oxidizing NADH and transferring electrons to the ubiquinone pool. Typically, Complex I mutants display a slow growth rate compared to wild-type plants. Here, using a forward genetic screen approach for restored growth of a Complex I mutant, we have identified the mitochondrial ATP-dependent metalloprotease, Filamentous Temperature Sensitive H 3 (FTSH3), as a factor that is required for the disassembly of Complex I. An ethyl methanesulfonate-induced mutation in FTSH3, named as *rmb1* (restoration of mitochondrial biogenesis 1), restored Complex I abundance and plant growth. Complementation could be achieved with FTSH3 lacking proteolytic activity, suggesting the unfoldase function of FTSH3 has a role in Complex I disassembly. The introduction of the *rmb1* to an additional, independent, and extensively characterized Complex I mutant, *ndufs4*, resulted in similar increases to Complex I abundance and a partial restoration of growth. These results show that disassembly or degradation of Complex I plays a role in determining its steady-state abundance and thus turnover may vary under different conditions.

Introduction

Protein abundance can be controlled at a variety of levels, from pre-transcriptional mechanisms (i.e. epigenetic) to protein degradation. In a variety of systems, it has been established that the rate of protein turnover varies greatly between proteins. Proteins with high regulatory functions exhibit high-turnover rates, which makes them responsive to changing conditions (Li et al., 2013, 2017; Szczepanowska et al., 2020). Whereas the ubiquitin–proteosome system is a well-established model for cytosolic protein degradation (Vierstra, 2009), the mechanisms involved in the turnover of organellar proteins remains poorly understood. It has been shown that chloroplast biogenesis is regulated by the ubiquitin–proteasome system (Ling et al., 2012) and that limited inhibition of cytosolic proteolysis leads to improvements in photosynthetic performance (Grimmer et al., 2020). As there is an inverse relationship between growth rate and protein turnover in *Arabidopsis thaliana* (Arabidopsis; Ishihara et al., 2017), the cost of translation and protein turnover may be an energy consuming

Received December 4, 2020. Accepted January 28, 2021. Advance access publication February 22, 2021

cycle that can be optimized to improve plant performance (Amthor et al., 2019).

Mitochondria undergo continuous changes to protein content in response to changing energetic demands or to replace misfolded, damaged, and aggregated proteins (Vazquez-Calvo et al., 2020). The matrix facing module of Complex I, known as the NQ-module, is particularly prone to oxidative damage as it contains a chain of eight iron–sulfur (Fe–S) clusters involved in electron transfer. In Arabidopsis and human (*Homo sapiens*), the N-module domain exhibits a rapid rate of turnover, up to six times higher than its membrane-bound counterparts (Li et al., 2017; Szczepanowska et al., 2020). This suggests that Complex I turnover is a highly regulated and selective process. The human mitochondrial matrix protease ClpXP is involved in the specific turnover of the matrix arm domain N-module (Szczepanowska et al., 2020). Interestingly, the N-module was found to dissociate from the membrane domain following oxidative phosphorylation (OXPHOS) impairment and subsequently degraded by ClpXP, a mitochondrial matrix protease consisting of the ClpX chaperone and the ClpP peptidase (Szczepanowska et al., 2020). This process of selected release is more energetically favorable than the disassembly, turnover, import, and reassembly of the full halo enzyme complex (Szczepanowska et al., 2020). In Arabidopsis, deletion of a related matrix protease subunit named caseinolytic protease subunit 2 resulted in the accumulation of the N-module sub complex within the matrix with no change to the Complex I halo enzyme abundance (Petereit et al., 2020). This suggests that the specific disassociation and rapid turnover of the N-domain module is a conserved mechanism for the removal of damaged Complex I subunits; however, the factors involved in this process are yet to be ascertained.

An Arabidopsis mitochondrial LYR-domain protein, named COMPLEX I ASSEMBLY FACTOR 1 (CIAF1), has been shown to be involved in the assembly of the NQ-module domain of Complex I (Ivanova et al., 2019). A T-DNA deletion mutant *ciaf1-1* exhibits low Complex I abundance due to a defect in the assembly of the NQ-module and a severe delayed growth phenotype. *ciaf1-1* is still capable of generating a fully functional Complex I and supercomplex I + III, but these are much reduced in abundance (Ivanova et al., 2019). To identify factors involved in plant Complex I biogenesis and turnover, we carried out a forward genetic screen approach. Ethyl methanesulfonate (EMS) mutagenesis was carried out on *ciaf1-1*. This mutant has much reduced Complex I abundance due to a defect in assembly and exhibits a severe delayed growth phenotype, like what has been observed for a variety of Complex I mutants (Meyer et al., 2011). A screen of the EMS population looked for restored growth to identify factors that may affect the turnover of Complex I. One EMS mutant identified was Filamentous Temperature Sensitive H 3 (FTSH3), a mitochondrial ATP-dependent metalloprotease, which displayed partial restoration of growth and Complex I abundance.

Results

Perturbation of individual Complex I subunits or assembly factors results in a decrease in Complex I abundance and activity resulting in plants with a retarded growth phenotype (Meyer et al., 2011). The retarded growth phenotype of Complex I mutants provides an excellent background for a forward genetic screen to identify revertants and thus factors that can regulate Complex I assembly and turnover. The *ciaf1-1* mutant (SALK_143656) was previously shown to contain a T-DNA insert within CIAF1, a Complex I assembly factor, and displays a delayed growth phenotype typical of Complex I-defective mutants (Figure 1, A and B; Ivanova et al., 2019). Furthermore, Complex I abundance is substantially decreased in *ciaf1-1* due to defective assembly of the matrix arm domain NQ-module (Ivanova et al., 2019). This mutant has been previously described to also contain a partial T-DNA insertion within the promotor of another gene, At1g72750 (Translocase of the Inner membrane; Tim23-2; Wang et al., 2012). To ensure that the observed retarded growth phenotype of *ciaf1-1* was only due to the T-DNA insertion within *ciaf1-1*, a filial cross was carried out with *ciaf1-1* and Col-0 and the segregating populations genotyped using PCR. The small, developmentally delayed phenotype was only observed in plants with the T-DNA within *CIAF1* and not within the promoter of At1g72750 (Tim23-2; Supplemental Figure S1). To identify factors involved in Complex I assembly and/or turnover, *ciaf1-1* seeds were treated with EMS and the M2 population visually screened for restoration of growth. A mutant that exhibited a substantial increase in plant growth and biomass relative to *ciaf1-1* was identified and the underlying mutation was identified and named *rmb1* for Restorationof Mitochondrial Biogenesis 1 (Figure 1A). This mutant, named *rmb1*::*ciaf1-1*, exhibited substantially improved plant growth rates compared to *ciaf1-1*. For example *rmb1*::*ciaf1-1* reached the developmental stage 1.10 (10 rosette leaves larger than 1 mm) at Day 21 compared to Day 26 for *ciaf1-1* when grown on Murashige and Skoog (MS) plate media (Figure 1Bi; Supplemental Table S2). Growth of *rmb1*::*ciaf1-1* on soil was similarly associated with improved growth, with *rmb1*::*ciaf1-1* reaching completion of flowering (stage 6.9) at Day 56 compared to Day 69 for *ciaf1-1*. In addition, *rmb1*::*ciaf1-1* exhibited significantly improved growth in parameters such as plant height, number of rosette leaves, rosette radius, and root length when compared to *ciaf1-1* at most time points (Figure 1B(iii); Supplemental Table S2; $P < 0.05$, Student's t test, $P < 0.05$, $n = 20$). Whole-genome sequencing on segregating homozygous populations identified a C to T mutation within At2g29080 (Figure 1C), which encodes for the mitochondrial FTSH3 protein. FTSH3 belongs to a highly conserved family of proteins found in mitochondria, chloroplasts, and bacteria that share a common membrane anchor domain, an AAA domain (ATPases Associated with a variety of cellular Activities), and a consensus metal-binding motif HEXGH that exhibits proteolytic activity (Gerdes et al., 2012). The mutation (proline to leucine) at residue 415 is

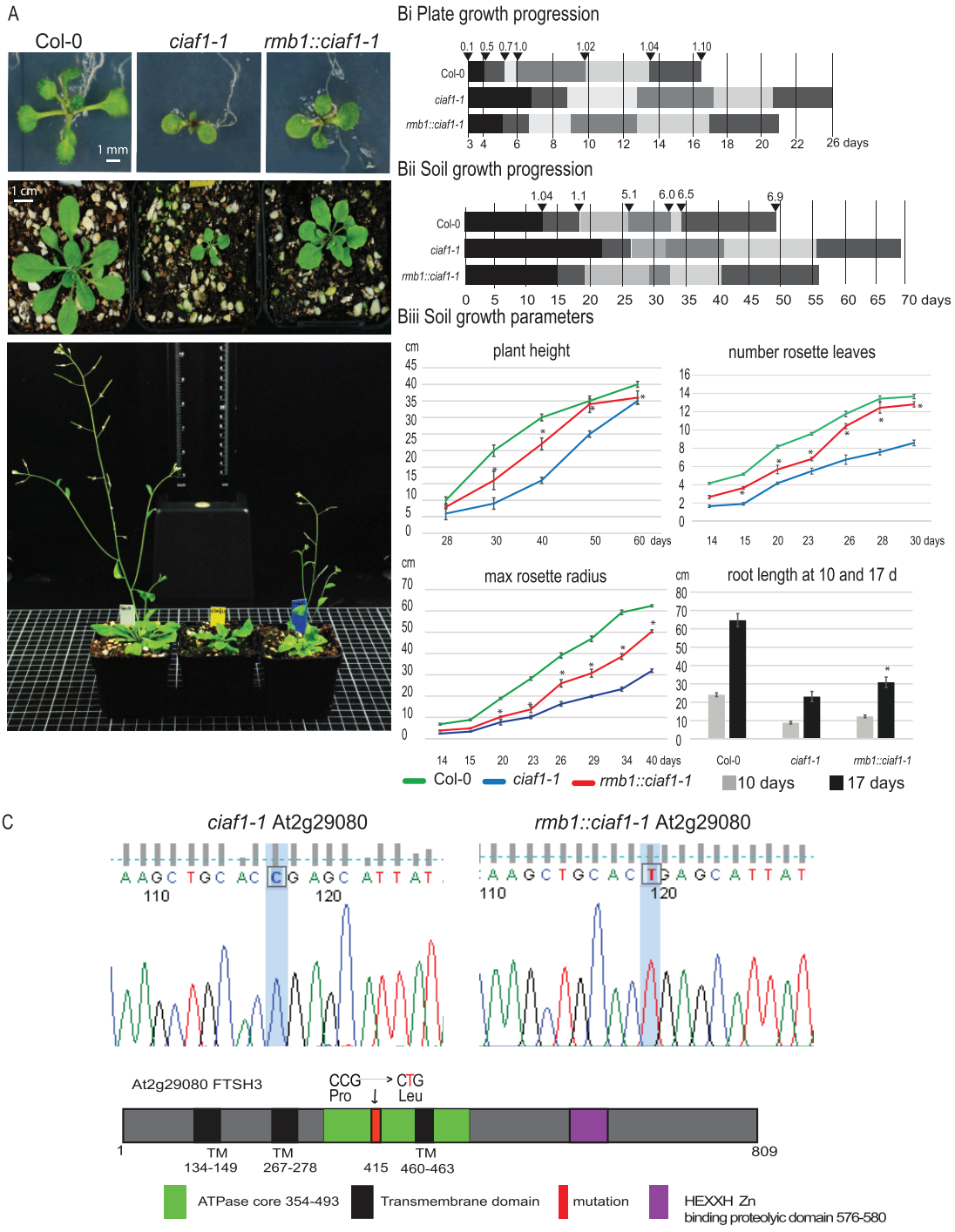

Figure 1 rmb1::*ciaf1-1* is an EMS mutant within FTSH3 that partially restores *ciaf1-1* developmental phenotype. A, The *ciaf1-1* mutant has a defect in mitochondrial respiratory Complex I assembly and consequently results in a small, developmentally delayed phenotype. An EMS forward genetic screen was carried out on *ciaf1-1* resulting in the identification of a mutant named *rmb1*::*ciaf1-1* (restoration of mitochondrial biogenesis 1) where plant growth was partially restored. B, Comprehensive stage growth progression analysis on plates (1.5% [w/v] sucrose MS media) (i) and soil (ii) indicates *rmb1*::*ciaf1-1* reached all growth stages earlier than *ciaf1-1*. Growth stages are as defined by Boyes et al. (2001). Analysis of growth parameters (iii) such as plant height, number of rosette leaves, rosette radius, and root length indicate *rmb1*::*ciaf1-1* performed significantly better than *ciaf1-1* ($p < 0.05$, Student's *t* test, $n = 20$). C, DNA sequencing confirmed that the mutation responsible for the phenotype was a C to T mutation with the At2g29080 gene. At2g29080 encodes for the mitochondrial AAA ATPase FTSH3 and the C to T mutation at amino acid 415 is within the chaperone ATPase domain. Scale bar = 1 cm.

within the predicted chaperone ATPase active domain of FTSH3 (Figure 1C).

To confirm that this mutation is responsible for the observed phenotype, a number of crosses and complementation lines were generated and characterized (Figure 2A). Since the mutation and phenotype was generated in the *ciaf1-1* background (*rmb1*::*ciaf1-1*), the *rmb1* mutation was also introduced into a Col-0 background (*rmb1*::Col-0) by filial crossing, with no significant alteration to plant phenotype observed (Figure 2A; Supplemental Figure S2 and Supplemental Table S2). A second allele for *rmb1* was obtained in the form of a FTSH3 T-DNA insertion line, *ftsh3-1* (SALK_037144), which did not show any phenotypic alterations (Figure 2A; Supplemental Figure S2 and Supplemental Table S2). This T-DNA line was cross-pollinated with *ciaf1-1* and double homozygous mutants were obtained to generate *ftsh3-1*::*ciaf1-1* (Figure 2A; Supplemental Figure S2 and Supplemental Table S2). *ftsh3-1*::*ciaf1-1* showed a substantial increase in plant growth when compared to the *ciaf1-1* mutant (Figure 2A; Supplemental Figure S2 and Supplemental Table S2). Stage growth progression analysis showed that *ftsh3-1*::*ciaf1-1* reached all developmental stages at the same time as *rmb1*::*ciaf1-1*, confirming that *rmb1/ftsh3.1* is responsible for the phenotypic reversion (Supplemental Figure S2 and Supplemental Table S2). To further confirm that the mutation within FTSH3 was responsible for the phenotypic reversion, a complementation line was generated whereby *rmb1*::*ciaf1-1* was transformed with the wild-type *FTSH3* gene under its native promoter (*rmb1*::proFTSH3). This line resulted in a reversion back to the small, developmentally delayed phenotype characteristic of the original EMS background *ciaf1-1*, confirming that the mutation within FTSH3 is the causative mutation for the restored plant growth of *rmb1*::*ciaf1-1* (Figure 2A; Supplemental Figure S2 and Supplemental Table S2). Transcript analysis confirmed *FTSH3* was expressed at normal levels in all lines except the *ftsh3-1* mutants (Supplemental Figure S3). Additionally, an overexpression line of FTSH3 was generated in a Col-0 background which showed $>$three-fold increase in FTSH3 protein abundance, but did not display any phenotypic alterations (Figure 2A; Supplemental Figures S2–S3).

To investigate Complex I abundance, mitochondria were isolated from all eight genotypes and analyzed by blue native polyacrylamide gel electrophoresis (BN-PAGE; Figure 2B). In-gel Complex I staining showed a significant increase to Complex I abundance in *rmb1*::*ciaf1-1* compared to *ciaf1-1* whereby the abundance of Complex I and I + III was restored by approximately two-fold (Figure 2B, $P < 0.05$, Student's t test). No significant change to Complex I abundance could be observed when *rmb1* was introduced into a Col-0 background (*rmb1*::Col-0) or when FTSH3 function was removed in Col-0 (*ftsh3-1*; Figure 2B). The double mutant line *ftsh3-1*::*ciaf1-1* also exhibited restored plant growth and a significant increase to Complex I abundance of approximately two-fold compared to *ciaf1-1* (Figure 2B). This suggests that the *ftsh3-1* deletion can restore Complex I abundance in the *ciaf1-1* background in a similar manner to the EMS *rmb1* mutation. Complementation of *rmb1*::*ciaf1-1* by the reintroduction of FTSH3 resulted in a decrease to Complex I abundance back to the levels as observed in *ciaf1-1* (Figure 2B).

To investigate the abundance of individual Complex I subunits within these lines, immunodetection was carried out on isolated mitochondria (Figure 2C). Immunodetection with antibodies raised against the Complex I inner membrane subunit B14.7 showed no obvious change in abundance in *ciaf1-1* and *rmb1*::*ciaf1-1* lines (Figure 2C). Similarly, no change to the abundance of the Complex I N-module subunits 75 kDa and 51 kDa could be observed. The carbonic anhydrase subunit GAMMA CARBONIC ANHYDRASE LIKE 1 (CAL1), a plant-specific Complex I subunit, also appeared unchanged in *rmb1*::*ciaf1-1* compared to *ciaf1-1* (Figure 2C). Blue Native Polyacrylamide Gel Electrophoresis (BN-PAGE) analysis clearly showed increased abundance of approximately two-fold of the monomeric Complex I and the Supercomplex I + III (Figure 2B), and therefore comprehensive proteomic analysis was carried out on rosette leaf tissue from Col-0, *ciaf1-1*, and *rmb1*::*ciaf1-1* (Figure 3). Very little change could be observed regarding the abundance of Complex I subunits, with only minor changes to the matrix arm domain subunits: 39, 23, 20, and 18 kDa increasing approximately 1.2- to 1.6-fold compared to *ciaf1-1* (Figure 3A; Supplemental Table S3).

Mapman representation of fold changes to the mitochondrial proteome similarly revealed minor change in *rmb1*::*ciaf1-1* compared to Col-0 and *ciaf1-1* compared to Col-0 (Figure 3B; Supplemental Table S3). Gene ontology (GO) enrichment analysis of whole tissue proteome revealed that the *ciaf1-1* mutant itself exhibits a substantial stress response when compared to Col-0 (Figure 3C) and that this response is mitigated in *rmb1*::*ciaf1-1*. Proteins annotated as GO term stress response were upregulated in *ciaf1-1* compared to Col-0, whereas general organellar activities and electron transfer chain (ETC) were constrained (Figure 3C, right panel). The mutation in *rmb1*::*ciaf1-1* normalized the expression of these stress-responsive proteins, including the WRKY transcription factors, CRK/LRR kinases, and heat-shock proteins (HSPs; Figure 3C). Furthermore, an improvement can be observed in the alternative ETC pathways as alternative oxidases (AOX) AOX1A/C and alternative NAD(P)H dehydrogenases (NDs) NDA1 and NDB2 are adjusted back to Col-0 levels (Figure 3C; Supplemental Table S3). Our proteomic analysis suggests that the abundances of FTSH3 proteolytic targets are not altered in *rmb1*::*ciaf1-1*. Furthermore, with only minor changes to the abundances of Complex I subunits, *rmb1*::*ciaf1-1* does not appear to exhibit defective proteolysis. To further demonstrate this, we transformed *rmb1*::*ciaf1-1* with FTSH3 devoid of its proteolytic function (*rmb1*::proFTSH3_TRAP; Figure 4) by changing a single amino acid (H to G at amino acid 586) in the proteolytic center. This leads to loss of proteolytic activity whilst

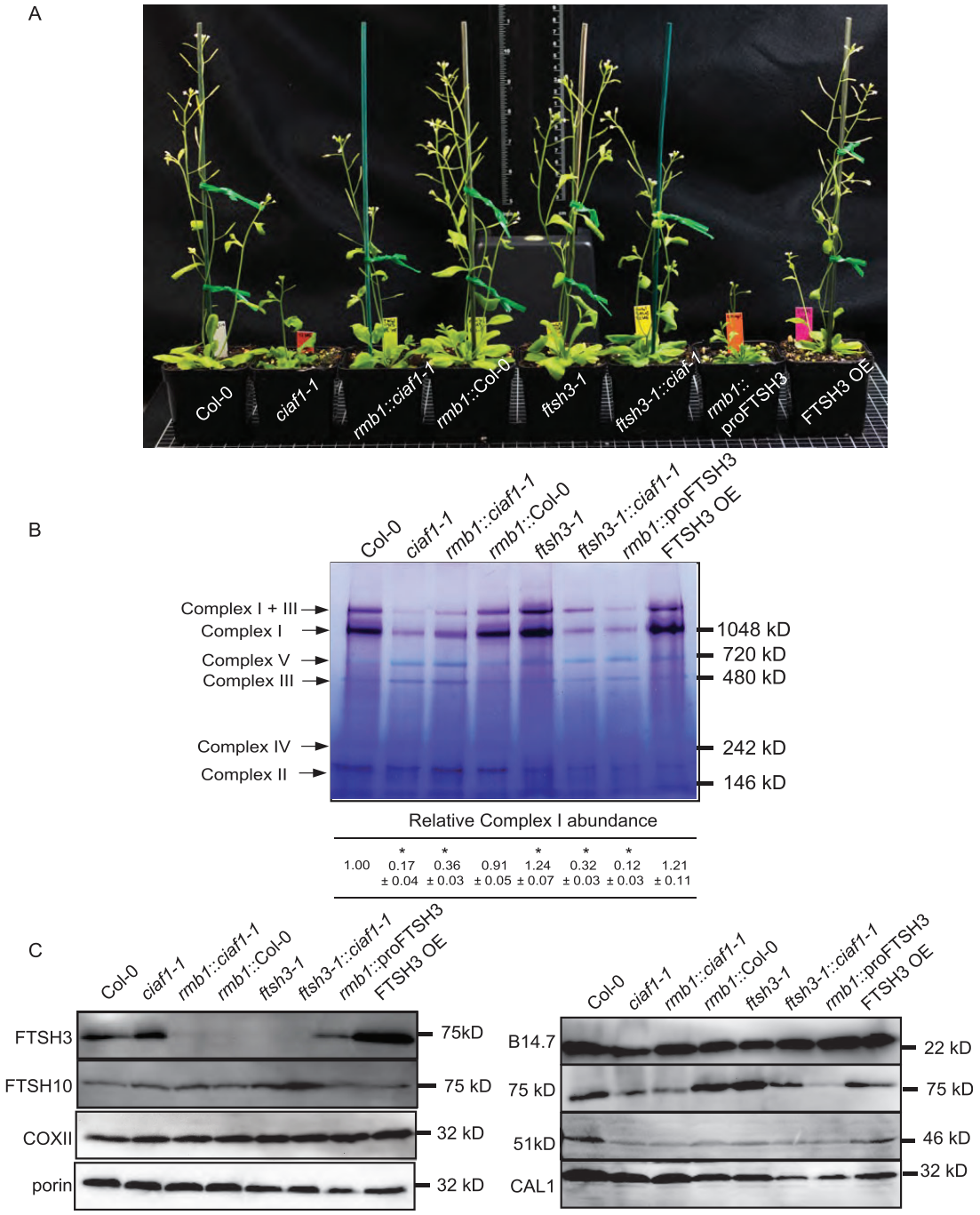

Figure 2 rmb1::*ciaf1-1* partially restored Complex I abundance and activity in *ciaf1-1*. A, Phenotypic analysis of Col-0, the Complex I mutant *ciaf1-1*, the EMS mutant *rmb1* in the *ciaf1-1* background (*rmb1*::*ciaf1-1*), *rmb1* in a Col-0 background (*rmb1*::Col-0), the FTSH3 T-DNA insertion line *ftsh3-1* (SALK_037144), *ftsh3-1* backcrossed to *ciaf1-1* (*ftsh3-1*::*ciaf1-1*), complemented *rmb1* (*rmb1*::proFTSH3), and a FTSH3 overexpressor (FTSH3 OE). B, Mitochondria were isolated from all lines and resolved by BN-PAGE and stained for Complex I abundance. The position of the major OXPHOS complexes is indicated on the left. Quantification averages of Complex I abundance relative to Col-0 are indicated below. Significant differences are indicated with a * (± SE, $p < 0.05$, Student's *t* test, $n = 3$). C, Mitochondria were isolated from all mutant lines and immunodetected with antibodies against FTSH3, its partner protein FTSH10, and mitochondrial controls COXII and porin. The abundance of Complex I subunits B14.7, 51 kDa, 75 kDa, and CAL were investigated showing little change in abundance across *ciaf1-1* and *rmb1*::*ciaf1-1*. Phenotypic data is presented in Supplemental Figure S2 and Supplemental Table S2.

the chaperone ATPase function is retained (Westphal et al., 2012; Lindemann et al., 2018; Opalinska et al., 2018; Adam et al., 2019; Kamal et al., 2019). *rmb1*::proFTSH3_TRAP plants displayed the small, developmentally delayed phenotype of *ciaf1-1* with stage 1.10 (10 rosette leaves >1 mm) being reached at 24–26 d compared to 16 d in Col-0 (Figures 4B and 2A; Supplemental Figure S3), similar to *rmb1*::*ciaf1-1* complemented with the fully functional FTSH3

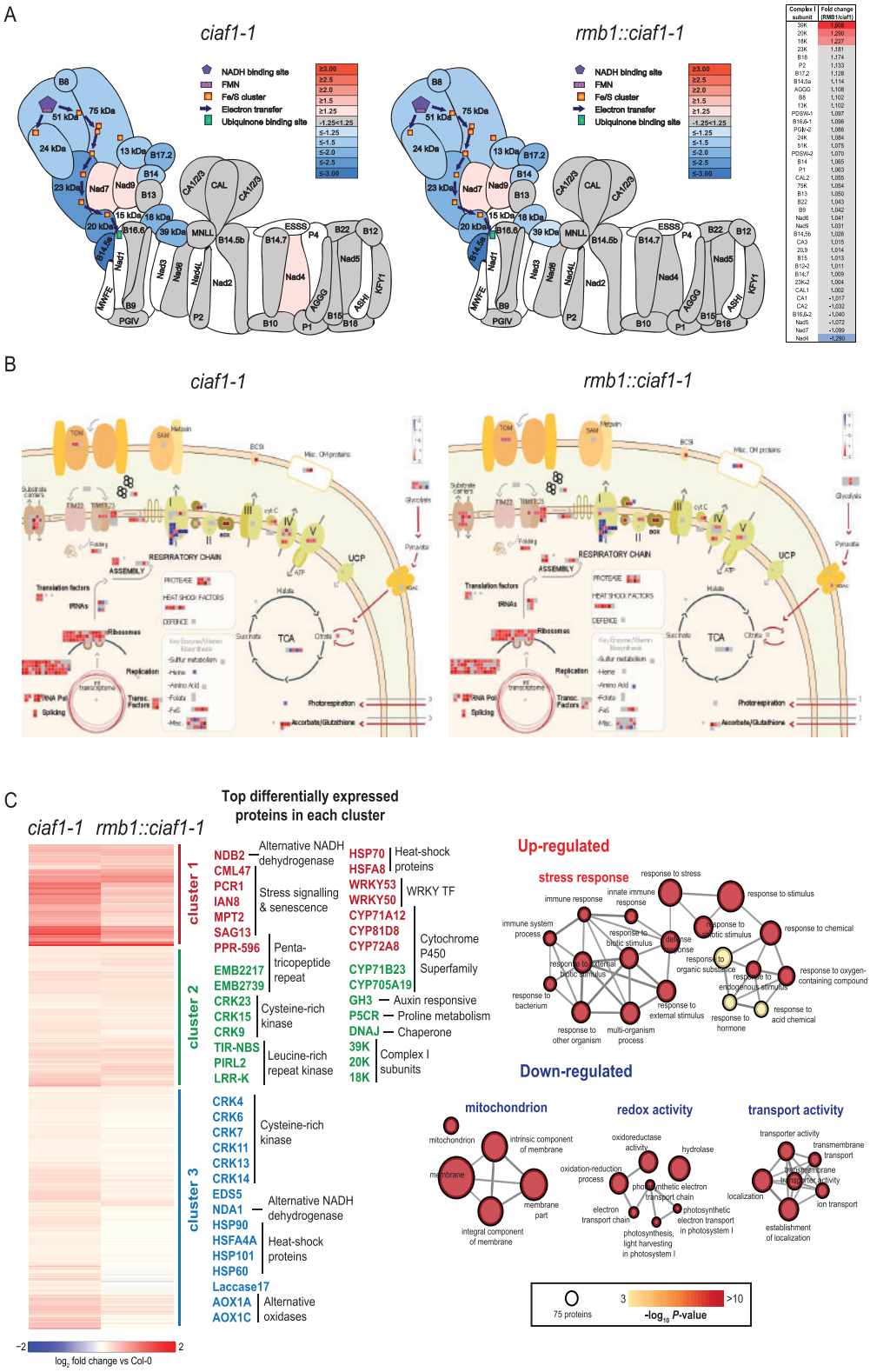

Figure 3 Proteomic analysis of *rmb1*::*ciaf1-1* shows no substantial alterations to Complex I abundance. HiRiEF LC/MS proteomics was carried out on Col-0, *ciaf1-1*, and *rmb1*::*ciaf1-1* rosette leaf tissue. A, Heatmap of Complex I subunits abundance fold change of *ciaf1-1* and *rmb1*::*ciaf1-1* compared to Col-0. Right-hand table shows fold-change of individual subunits in *rmb1* compared to *ciaf1-1*, with a notable restoration on 39 kDa, 20 kDa, and 18 kDa subunits (see Supplemental Table S2 for data). B, Mapman visualization of fold changes of mitochondrial proteins in *ciaf1-1* and *rmb1*::*ciaf1-1* compared to Col-0. C, Left: heatmap of differentially expressed proteins in *ciaf1-1* and *rmb1*::*ciaf1-1* after Euclidian distribution and hierarchical clustering using Ward method (left-hand heatmap), showing a restoration of proteins mainly associated with stress response in all clusters (right-hand list). Right: GO term enrichment analysis of up- and downregulated proteins in *ciaf1-1* compared to Col-0. The size of nodes represents the number of proteins in each GO term and the color represents the corresponding $-\log_{10}$ *P*-value for enrichment after Bonferroni correction. Full proteomic changes are listed in Supplemental Table S3.

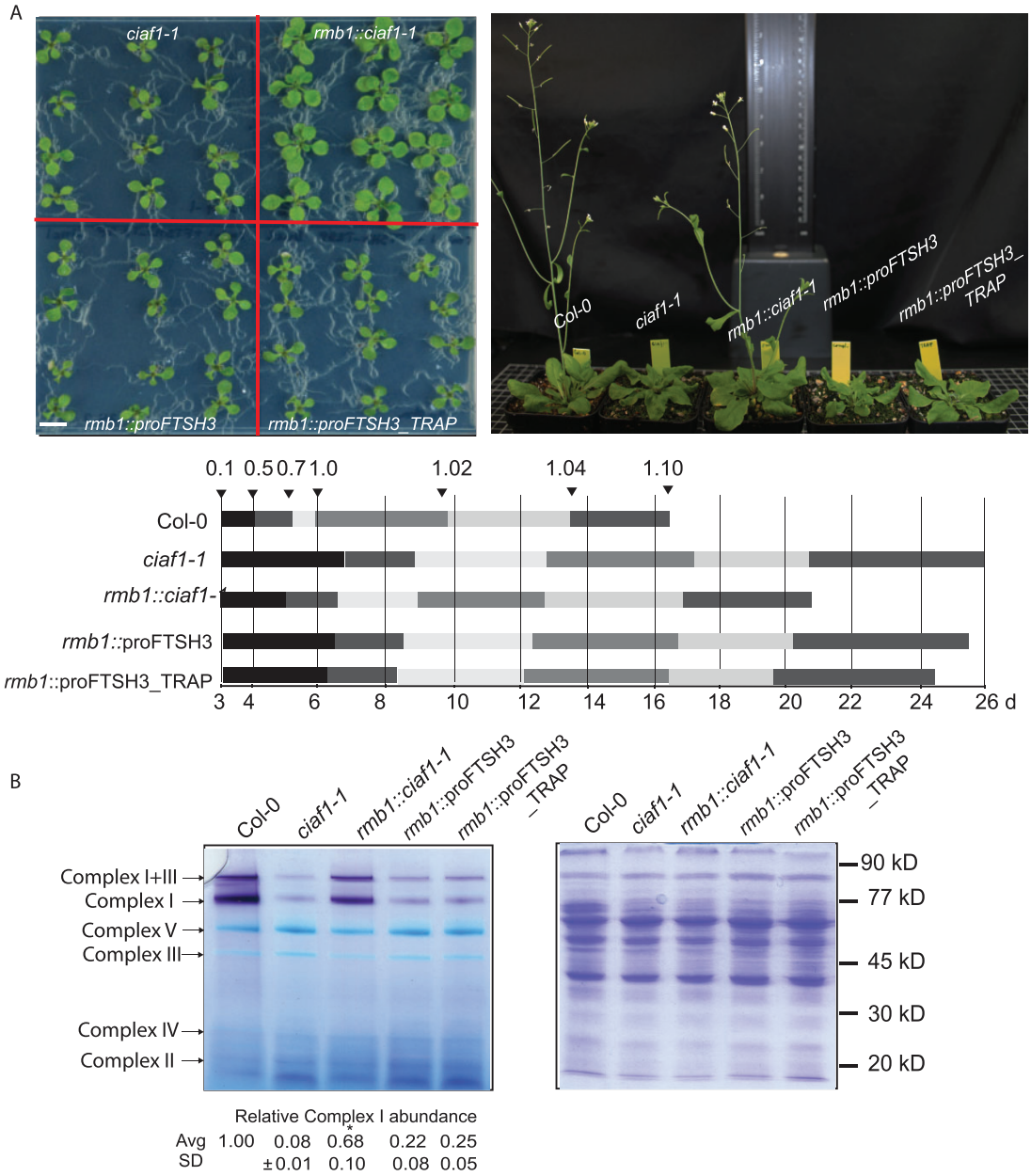

Figure 4 Complementation of *rmb1*::*ciaf1-1* with a proteolytic defective FTSH3. A, Complementation of *rmb1*::*ciaf1-1* with FTSH3 (*rmb1*::*proFTSH3*) results in the reversion back to the small, developmental delayed phenotype of *ciaf1-1*. Complementation of *rmb1*::*ciaf1-1* with FTSH3 where the proteolytic domain has been inactivated (*rmb1*::*proFTSH3_TRAP*) similarly results in a reversion of phenotype suggesting that the proteolytic domain is not required to achieve complementation. Scale bar = 1 cm. B, Mitochondria were isolated from all lines and resolved by BN-PAGE and stained for Complex I abundance. The position of OXPHOS complexes are indicated on the left. Quantification of Complex I and I + III abundances relative to Col-0 are indicated below. Significant differences are indicated with an asterisk (±SD, $P < 0.05$, Student's *t* test, $n = 3$). A Coomassie stain of total mitochondrial protein resolved by SDS–PAGE is shown on the right.

(*rmb1*::proFTSH3). Mitochondria were isolated from these lines and Complex I abundance determined by BN-PAGE and Complex I staining (Figure 4C). Complementation of *rmb1*::*ciaf1-1* with FTSH3 and FTSH3_TRAP results in Complex I abundance decreasing from 68% to 22% (*rmb1*::proFTSH3) and 25% (*rmb1*::proFTSH3_TRAP; Figure 4C). This demonstrates that *rmb1*::*ciaf1-1* complementation was achieved without the proteolytic domain, suggesting the chaperone ATPase domain of FTSH3 plays a role in regulating Complex I abundance in these mutant lines.

To investigate if FTSH3 can regulate Complex I abundance and restore growth in other Complex I mutants, an additional double mutant line was generated (Figure 5). NDUFS4 (18 kDa) Complex I subunit has been previously proposed to be involved in Complex I stability and/or assembly rather than electron transfer (Kruse et al., 2008; Breuer et al., 2013;

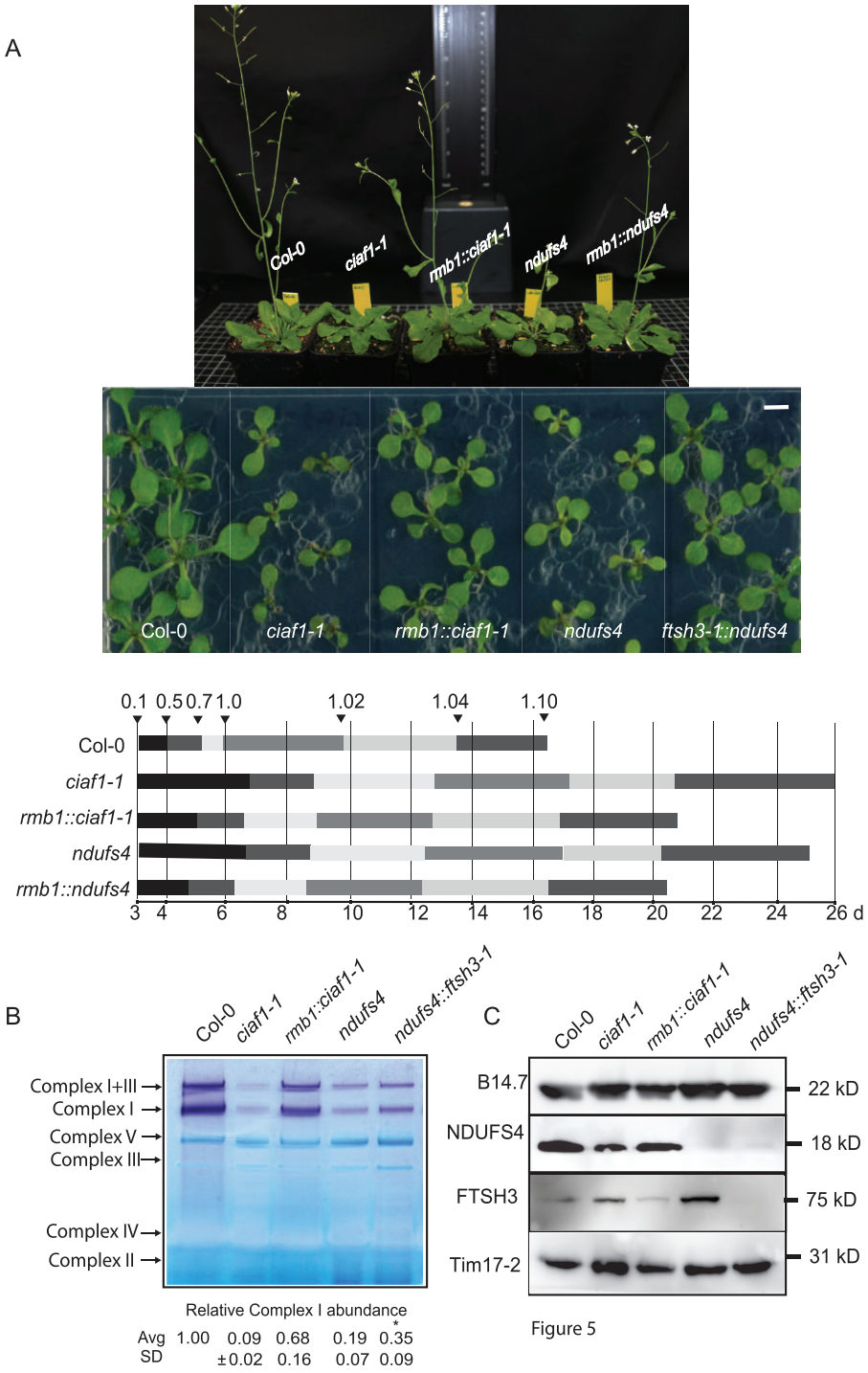

Figure 5

Figure 5 The deletion of FTSH3 can restore Complex I abundance in an independent Complex I deletion mutant. A, *ndufs4* is a T-DNA insertion knockout line within the Complex I subunit NDUFS4 (SAIL_596_E11; Meyer et al. 2009) that exhibits a substantial loss of Complex I abundance and activity. A filial cross between *ftsh3-1* (SALK_037144) and *ndufs4* resulted in plants that display an increased growth phenotype, as observed with *rmb1*::*ciaf1-1*. B, Mitochondria were isolated from all lines, resolved by BN-PAGE, and stained for Complex I abundance. The positions of OXPHOS complexes are indicated on the left. Quantification averages of Complex I and I + III abundance are indicated below. Significant differences are indicated with an asterisk (±SD, $P < 0.05$, Student's *t* test, $n = 3$). C, Immunodetection of isolated mitochondria with antibodies against the Complex I subunits B14.7 and NDUFS4, FTSH3, and Tim17-2.

Kahlhofer et al., 2017). Deletion of this subunit results in small, developmentally delayed plants that display a substantial loss of Complex I abundance (Meyer et al., 2009). To determine if FTSH3 plays a role in regulating Complex I abundance in *ndufs4*, a *ftsh3.1*::*ndufs4* double mutant line was generated (Figure 5). This double mutant showed a substantial increase to plant growth when compared to *ndufs4* and *ciaf1-1* (Figure 5A). *ftsh3.1*::*ndufs4* was able to reach

stage 1.10 (10 rosette leaves > 1 mm) at Day 20.5 compared to Day 25 for *ndufs4*; *ftsh3.1*::*ndufs4* reached all stages earlier suggesting a restoration of Complex I abundance (Figure 5B). Mitochondrial isolation and BN-PAGE indeed revealed a significant restoration to Complex I abundance from 19% in *ndufs4* to 35% in *ftsh3.1*::*ndufs4* relative to Col-0 (Figure 5B, $P < 0.05$, Student's t test). Immunodetection of isolated mitochondria from all lines showed no change to the abundance of the Complex I subunit B14.7 (Figure 5C), whereas immunodetection of NDUFS4 and FTSH3.1 confirmed at a protein level that NDUFS4 and FTSH3 are not present, and Tim17-2 confirmed equal loading (Figure 5C). These results indicate that the abundance of Complex I in affected by FTSH3 in independent Complex I-defective backgrounds.

Discussion

Here, we have characterized a role for FTSH3 in regulating Complex I abundance. Our data shows that a mutation within the chaperone AAA domain of FTSH3, or a deletion of FTSH3 has allowed Complex I to accumulate in two independent Complex I-defective backgrounds. The FTSH3 protein belongs to the FTSH family of proteins. These proteases are embedded within plasma membranes, inner mitochondrial membranes, or chloroplast thylakoids via an anchor domain at the N-terminus. FTSH proteins contain a chaperone/unfoldase AAA domain (ATPases Associated with a variety of cellular Activities) and a consensus metal-binding motif that exhibits proteolytic activity (Gerdes et al., 2012; Langklotz et al., 2012). The mutation within the chaperone/unfoldase AAA domain of FTSH3 resulted in an accumulation of Complex I within *ciaf1-1*, a Complex I-defective mutant. Proteomic analysis failed to identify any proteolytic targets suggesting that the accumulation of Complex I was likely achieved via a defect in the unfolding and disassembly of Complex I, rather than proteolysis of individual Complex I subunits. This hypothesis was further confirmed by the observation that the proteolytic-defective FTSH3 (FTSH3_TRAP) was able to complement *rmb1*::*ciaf1-1*. The role of FTSH3 in regulating Complex I abundance could also be revealed in the *ndufs4* mutant. NDUFS4 has been proposed to be involved in maintaining Complex I structural integrity, and in *ndufs4*, Complex I subunits are being transcribed, translated, and imported normally with all membrane assembly submodules generated (Wang et al., 2012; Meyer et al., 2009, 2011; Kuhn et al., 2015). The inability to identify N-module subunits in *ndufs4* (Kuhn et al., 2015) suggests an assembly defect and/or an unstable structure. Recent cryo EM structures of plant Complex I show NDUFS4 situated on the peripheral end of the N-module (Maldonado et al., 2020; Soufari et al., 2020), supporting a structural maintenance role and that the lack of Complex I in *ndufs4* is likely due to rapid turnover of an unstable Complex I. Here, we have shown that defective FTSH3 within the *ndufs4* background results in an increased accumulation of Complex I and increased plant growth. This suggests that in both mutants, FTSH3 plays a role in the disassembly of Complex I and thus FTSH3 inactivation results in Complex I accumulation.

FTSH3 proteins have been well characterized in a number of species and a common theme shows the AAA domain is essential for the unfolding of substrates and the translocation to its proteolytic site (Tatsuta and Langer, 2009; Gerdes et al., 2012; Quiros et al., 2015). Interestingly, it has also been reported that the AAA domain can have a chaperone/unfoldase role independent to proteolysis. Membrane-bound OXPHOS subunits were found to be actively removed by AAA proteases, independent to proteolytic activity (Tatsuta and Langer, 2009; Gerdes et al., 2012; Zurita Rendon and Shoubridge, 2012; Quiros et al., 2015). The AAA domain can mediate interactions with select membrane proteins for further degradation either by itself or by other mitochondrial proteases (Leonhard et al., 1999; Tatsuta et al., 2007; Botelho et al., 2013). For example, in yeast (*Saccharomyces cerevisiae*) mitochondria, the cytochrome *c* peroxidase (Ccp1) precursor protein is specifically released from the inner membrane via the matrix-facing m-AAA protease prior to proteolysis by a rhomboid protease (Tatsuta et al., 2007). A chaperone activity has also been identified for aggregated inner membrane proteins whereby the yeast FTSH Yme1 is able to prevent the formation of intermembrane space aggregates by protein refolding rather than proteolysis (Leonhard et al., 1999; Schreiner et al., 2012).

Arabidopsis FTSH3 has been previously characterized and also shown to exhibit both chaperone and unfoldase functions (Kolodziejczak et al., 2018). Arabidopsis FTSH3 was shown to process yeast MrpL32, a mitochondrial ribosomal subunit (Nolden et al., 2005; Kolodziejczak et al., 2018). FTSH3 is also able to dislocate the yeast Ccp1 precursor protein from the inner membrane (Kolodziejczak et al., 2018), showing that the chaperone and unfoldase functions of FTSH3 proteins are conserved in plants (Voos, 2013). Here, we have identified an additional chaperone role for FTSH3 with regards to regulating Complex I abundance. Whereas our protein analysis did not identify any clear proteolytic substrates for FTSH3, we did observe a small increase in the 39, 20, 18, and 23 kDa subunits in the EMS mutant. Interestingly these subunits have been shown to sit between the membrane and matrix arm NQ-module in Arabidopsis (Ligas et al., 2019), which raises the possibility that FTSH3 exerts its function on potential NQ-module anchoring proteins, facilitating their disassociation and proteolysis.

No changes to plant growth were observed in either *rmb1* or *ftsh3-1* in a Col-0 background. A significant increase in Complex I abundance was observed in *ftsh3-1* (1.2-fold increase). A similar significant increase was also observed in the FTSH3 overexpressing line, suggesting that additional mechanisms exist to regulate the abundance of Complex I, or that other components can compensate for the loss of FTSH3 in wild-type backgrounds. Arabidopsis FTSH3 is known to exist as homo- or hetero-oligomers, with FTSH10 forming a large supramolecular structure (Steglich et al.,

1999; Piechota et al., 2010). Deletion of both FTSH3 and FTSH10 *in planta* resulted in slower rates of mitochondrial translation (likely due to their role in MrpL32 proteolysis) with surprisingly no impact to plant growth phenotype (Kolodziejczak et al., 2018). Mitochondria contain additional FTSH proteases, FTSH4 and FTSH11, termed as i-AAA proteases, with their proteolytic domain facing the intermembrane space (Urantowka et al., 2005). Both FTSH4/11 have been linked to regulating the abundance of Complex I, II, III, and V subunits (Zhang et al., 2014a, 2014b), plant stress, and autophagy (Zhang et al., 2017). Further, FTSH4 has been linked to maintaining cardiolipin content (Smakowska et al., 2016), a known regulator of Complex I activity (Jussupow et al., 2019). Targeted multiple reaction monitoring mass spectrometry of *ftsh4* has identified potential substrates in several Complex II subunits during seed germination (Heidorn-Czarna et al., 2018). Consequently, it is becoming clear that FTSH proteins have many diverse roles in maintaining mitochondrial homeostasis, in particular with respect to the OXPHOS machinery. This study raises an interesting question of what signals the degradation of protein or complexes and how the activities of FTSH proteins are activated or regulated. The identification of the triggers for protein degradation and the machinery involved in protein turnover provide further targets to regulate plant growth, processes that have the potential for optimization via optimized resource allocation (Amthor et al., 2019).

Materials and methods

Plant growth and phenotyping

Col-0 (*cv* Columbia-0), EMS mutants, and T-DNA insertional mutants were germinated on 0.5 MS salt medium containing 1.5% (w/v) sucrose and grown at 22°C with a light intensity of 80 µmol quanta m^2 s in a 16-h photoperiod. The SALK T-DNA insertion line *ftsh3.1* (SALK_037144) was obtained from the ABRC seed stock center (Alonso et al., 2003). *ndufs4* (SAIL_596_E11) was obtained from E. Meyer (Meyer et al., 2009). Mutant lines were screened for homozygosity of the T-DNA insert with the primers listed in Supplemental Table S1 according to SALK Institute T_DNA Arabidopsis mapping tool suggestions. Genomic DNA was isolated from 14-d-old plants, and PCR was performed using the MyFi Mix (Bioline) according to the manufacturer's instructions. Plant phenotyping was performed according to the parameters as described previously (Boyes et al., 2001). Student's *t* test ($P < 0.05$) was used to determine any significant differences between Col-0 and mutants.

EMS mutagenesis and forward genetic screen

EMS mutagenesis was carried out on the seeds of the *ciaf1-1* homozygous line (SALK_143656) according to parameters as described previously (Weigel and Glazebrook, 2006; Ivanova et al., 2019). A visual screen of EMS mutants was carried out to identify plants with increased growth compared to *ciaf1-1*. Approximately 2,000 individual M2 plants were grown and screened on MS media. Candidate revertant lines were phenotypically confirmed as true mutants in the subsequent M3 generations following at least three rounds of backcrossing to *ciaf1-1*.

Whole-genome sequencing and mapping

Whole-genome sequencing using the Illumina HiSeq 2500 was carried out in six individual homozygous lines. Sequencing libraries were generated from isolated genomic DNA (QIAGEN DNeasy MAXI kit) using the Nextera DNA Flex Library Prep Kit according to the manufacture (Illumina). Libraries were sequenced with a 70-bp read length on a NextSeq500 system (Illumina). Reads were aligned to the Arabidopsis reference genome (Araport11) with bowtie2 v2.3.4.1 (Langmead and Salzberg, 2012) and mutations identified using the "mpileup" and "call" commands of bcftools v1.4 using standard parameters (http://www.htslib.org/doc/bcftools.html). A single nucleotide polymorphism at position 12,491,285 on Chromosome 2, C to T, was present in all six homozygous mutant lines within the coding region of At2g29080.

Generation of constructs

Cloning from cDNA was performed using the HiFi Mix (Bioline) according to the manufacturer's instructions using primers listed in Supplemental Table S1. cDNA was amplified using gene-specific primers flanked by Gateway™ recombination cassettes and cloned into pDONR201 and recombined into B2GW7 for *Agrobacterium tumefaciens*-mediated transformation to generate the overexpression line (Karimi et al., 2002). The full-length *FTSH3* gene (At2g28090) including the 1-kb upstream promoter region was amplified from Col-0 genomic DNA using primers listed in Supplemental Table S1 and cloned into pCAMBIA1300 using NEBuilder HiFi DNA Assembly Master Mix (BioLabs) according to the manufacturer's instructions. Site Directed Mutagenesis was carried out using Stratagene's QuikChange™ mutagenesis kit with primers listed in Supplemental Table S1.

Reverse transcription quantitative PCR

Total RNA from 14-d-old seedlings was extracted using FavorPrep Plant Total RNA Purification Mini Kit according to the manufacturer's instructions (FAVORGEN Biotech Corp). RcDNA was generated using HighCapacity cDNA Reverse Transcription Kit (Applied Biosystems) according to manufacturer's instructions. RT-qPCR was performed using the Light Cycler (Roche Applied Science) and 2xPCR master SYBR mix (Roche Applied Science).

Mitochondrial isolation, immunodetection, blue native PAGE, and activity staining

Mitochondria were isolated from 10-d-old seedlings grown in water pots as described previously (Duncan et al., 2015). Immunodetection was carried out using antibodies raised against FTSH3 (AGRISERA), COXII (AGRISERA), B14.7 (Wang et al., 2012), Tim17-2 (Murcha et al., 2005), 51 kDa (PhytoAb, USA), 75 kDa (PhytoAb, USA), CAL1 (Fromm et al., 2016), and NDUFS4 (Meyer et al., 2009). Quantification of FTSH3 was carried out using ImageQuant™ (GE

Healthcare Life Sciences). BN-PAGE was carried out as described previously (Eubel et al., 2005) using 5% (w/v) digitonin and precast 4%–16% Bis–Tris Gels (NOVEX). In-gel Complex I staining was carried out as described by Schertl and Braun (2015). Quantification of FTSH3 and Complex I abundance was carried out using ImageJ software (Schneider et al., 2012).

Proteomic analysis

HiRiEF High resolution isoelectric focusing (HiRIEF) liquid chromatography–mass spectrometry (LC-MS) proteomics was carried out as described previously (Branca et al., 2014; Ivanova et al., 2019) and data deposited online at the ProteomeXchange Consortium via the PRIDE partner repository with the dataset identifier PXD011795. Detected proteins were filtered for significant differences in *ciaf-1* and *rmb1*::*ciaf1-1* compared to Col-0. Protein levels were considered significantly different when $P < 0.05$ and absolute value of $\log_2$ fold-change > 0.25 (Kmiec et al., 2018). Heatmap of differentially expressed proteins was generated in R using Euclidean distribution metric ad hierarchical clustering with ward distance method. GO term enrichment analysis was performed with two-sided hypergeometric enrichment test and Bonferroni *P*-value correction using ClueGO plugin in Cytoscape (Bindea et al., 2009).

Accession numbers

Actin2 (At3g18780), CIAF1-1 (At1g76060), FTSH3 (At2g28900), FTSH10 (At1g07510), COXII (At2g07695), porin (At3g01280), B14.7 (At2g42210), 75 kDa (At5g37510), 51 kDa (At5g08530), CAL1 (At5g63510), NDUFS4 (At5g67590). Tim17-2 (At2g37410) and Tim23-2 (At1g72750).

Supplemental data

The following materials are available in the online version of this article.

Supplemental Figure S1. Segregation of SALK_14656 that contains two T-DNA insertions, one within CIAF1-1 and another 300-bp fragment within the promoter of At1g72750.

Supplemental Figure S2. Phenotypic analysis of Col-0, *ciaf1-1*, *rmb1*::*ciaf1-1*, crosses, and complemented lines.

Supplemental Figure S3. Confirmation of mutant lines used in this study.

Supplemental Table S1. Primers used in this study.

Supplemental Table S2. Phenotyping data.

Supplemental Table S3. Protein abundance changes in *ciaf1-1* and *rmb1*::*ciaf1-1*.

Funding

M.W.M. was supported by Australian Research Council (ARC) Future Fellowship FT130100112. A.S.G. was supported by Australian Government International Research Training Program and University Postgraduate Award at the University of Western Australia. J.W. was supported by the Australian Research Council Centre of Excellence in Plant Energy Biology (CE140100008).

Conflict of interest statement. None declared.

References

Adam Z, Aviv-Sharon E, Keren-Paz A, Naveh L, Rozenberg M, Savidor A, Chen J (2019) The chloroplast envelope protease FTSH11 – interaction with CPN60 and identification of potential substrates. Front Plant Sci **10**: 428

Alonso JM, Stepanova AN, Leisse TJ, Kim CJ, Chen H, Shinn P, Stevenson DK, Zimmerman J, Barajas P, Cheuk R, et al. (2003) Genome-wide insertional mutagenesis of Arabidopsis thaliana. Science **301**: 653–657

Amthor JS, Bar-Even A, Hanson AD, Millar AH, Stitt M, Sweetlove LJ, Tyerman SD (2019) Engineering strategies to boost crop productivity by cutting respiratory carbon loss. Plant Cell **31**: 297–314

Bindea G, Mlecnik B, Hackl H, Charoentong P, Tosolini M, Kirilovsky A, Fridman WH, Pages F, Trajanoski Z, Galon J (2009) ClueGO: a Cytoscape plug-in to decipher functionally grouped gene ontology and pathway annotation networks. Bioinformatics **25**: 1091–1093

Boyes DC, Zayed AM, Ascenzi R, McCaskill AJ, Hoffman NE, Davis KR, Gorlach J (2001) Growth stage-based phenotypic analysis of Arabidopsis: a model for high throughput functional genomics in plants. Plant Cell **13**: 1499–1510

Branca RM, Orre LM, Johansson HJ, Granholm V, Huss M, Perez-Bercoff A, Forshed J, Kall L, Lehtio J (2014) HiRIEF LC-MS enables deep proteome coverage and unbiased proteogenomics. Nat Methods **11**: 59–62

Breuer ME, Willems PH, Smeitink JA, Koopman WJ, Nooteboom M (2013) Cellular and animal models for mitochondrial complex I deficiency: a focus on the NDUFS4 subunit. IUBMB Life **65**: 202–208

Botelho SC, Tatsuta T, von Heijne G, Kim H (2013) Dislocation by the m-AAA protease increases the threshold hydrophobicity for retention of transmembrane helices in the inner membrane of yeast mitochondria. J Biol Chem **288**: 4792–4798

Duncan O, Carrie C, Wang Y, Murcha MW (2015) In vitro and in vivo protein uptake studies in plant mitochondria. Methods Mol Biol **1305**: 61–81

Eubel H, Braun HP, Millar AH (2005) Blue-native PAGE in plants: a tool in analysis of protein-protein interactions. Plant Methods **1**: 11

Fromm S, Senkler J, Eubel H, Peterhansel C, Braun HP (2016) Life without complex I: proteome analyses of an Arabidopsis mutant lacking the mitochondrial NADH dehydrogenase complex. J Exp Bot **67**: 3079–3093

Gerdes F, Tatsuta T, Langer T (2012) Mitochondrial AAA proteases–towards a molecular understanding of membrane-bound proteolytic machines. Biochim Biophys Acta **1823**: 49–55

Grimmer J, Helm S, Dobritzsch D, Hause G, Shema G, Zahedi RP, Baginsky S (2020) Mild proteasomal stress improves photosynthetic performance in Arabidopsis chloroplasts. Nat Commun **11**: 1662

Heidorn-Czarna M, Domanski D, Kwasniak-Owczarek M, Janska H (2018) Targeted proteomics approach toward understanding the role of the mitochondrial protease FTSH4 in the biogenesis of OXPHOS during Arabidopsis seed germination. Front Plant Sci **9**: 821

Ishihara H, Moraes TA, Pyl ET, Schulze WX, Obata T, Scheffel A, Fernie AR, Sulpice R, Stitt M (2017) Growth rate correlates negatively with protein turnover in Arabidopsis accessions. Plant J **91**: 416–429

Ivanova A, Gill-Hille M, Huang S, Branca RM, Kmiec B, Teixeira PF, Lehtio J, Whelan J, Murcha MW (2019) A mitochondrial LYR protein is required for Complex I assembly. Plant Physiol **181**: 1632–1650

Jussupow A, Di Luca A, Kaila VRI (2019) How cardiolipin modulates the dynamics of respiratory complex I. Sci Adv **5**: eaav1850

Kahlhofer F, Kmita K, Wittig I, Zwicker K, Zickermann V (2017) Accessory subunit NUYM (NDUFS4) is required for stability of the electron input module and activity of mitochondrial complex I. Biochim Biophys Acta Bioenerg **1858**: 175–181

Kamal SM, Rybtke ML, Nimtz M, Sperlein S, Giske C, Trcek J, Deschamps J, Briandet R, Dini L, Jansch L, et al. (2019) Two FtsH proteases contribute to fitness and adaptation of Pseudomonas aeruginosa Clone C Strains. Front Microbiol **10**: 1372

Karimi M, Inze D, Depicker A (2002) GATEWAY vectors for Agrobacterium-mediated plant transformation. Trends Plant Sci **7**: 193–195

Kmiec B, Branca RMM, Berkowitz O, Li L, Wang Y, Murcha MW, Whelan J, Lehtio J, Glaser E, Teixeira PF (2018) Accumulation of endogenous peptides triggers a pathogen stress response in Arabidopsis thaliana. Plant J **96**: 705–715

Kolodziejczak M, Skibior-Blaszczyk R, Janska H (2018) m-AAA complexes are not crucial for the survival of arabidopsis under optimal growth conditions despite their importance for mitochondrial translation. Plant Cell Physiol **59**: 1006–1016

Kruse SE, Watt WC, Marcinek DJ, Kapur RP, Schenkman KA, Palmiter RD (2008) Mice with mitochondrial complex I deficiency develop a fatal encephalomyopathy. Cell Metab **7**: 312–320

Kuhn K, Obata T, Feher K, Bock R, Fernie AR, Meyer EH (2015) Complete mitochondrial Complex I deficiency induces an up-regulation of respiratory fluxes that is abolished by traces of functional Complex I. Plant Physiol **168**: 1537–1549

Langklotz S, Baumann U, Narberhaus F (2012) Structure and function of the bacterial AAA protease FtsH. Biochim Biophys Acta **1823**: 40–48

Langmead B, Salzberg SL (2012) Fast gapped-read alignment with Bowtie 2. Nat Methods **9**: 357–359

Leonhard K, Stiegler A, Neupert W, Langer T (1999) Chaperone-like activity of the AAA domain of the yeast Yme1 AAA protease. Nature **398**: 348–351

Li L, Nelson CJ, Carrie C, Gawryluk RM, Solheim C, Gray MW, Whelan J, Millar AH (2013) Subcomplexes of ancestral respiratory complex I subunits rapidly turn over in vivo as productive assembly intermediates in Arabidopsis. J Biol Chem **288**: 5707–5717

Li L, Nelson CJ, Trosch J, Castleden I, Huang S, Millar AH (2017) Protein degradation rate in Arabidopsis thaliana leaf growth and development. Plant Cell **29**: 207–228

Ligas J, Pineau E, Bock R, Huynen MA, Meyer EH (2019) The assembly pathway of complex I in Arabidopsis thaliana. Plant J **97**: 447–459

Lindemann C, Thomanek N, Kuhlmann K, Meyer HE, Marcus K, Narberhaus F (2018) Next-generation trapping of protease substrates by label-free proteomics. Methods Mol Biol **1841**: 189–206

Ling Q, Huang W, Baldwin A, Jarvis P (2012) Chloroplast biogenesis is regulated by direct action of the ubiquitin-proteasome system. Science **338**: 655–659

Maldonado M, Padavannil A, Zhou L, Guo F, Letts JA (2020) Atomic structure of a mitochondrial complex I intermediate from vascular plants. Elife **9**

Meyer EH, Solheim C, Tanz SK, Bonnard G, Millar AH (2011) Insights into the composition and assembly of the membrane arm of plant complex I through analysis of subcomplexes in Arabidopsis mutant lines. J Biol Chem **286**: 26081–26092

Meyer EH, Tomaz T, Carroll AJ, Estavillo G, Delannoy E, Tanz SK, Small ID, Pogson BJ, Millar AH (2009) Remodeled respiration in ndufs4 with low phosphorylation efficiency suppresses Arabidopsis germination and growth and alters control of metabolism at night. Plant Physiol **151**: 603–619

Murcha MW, Millar AH, Whelan J (2005) The N-terminal cleavable extension of plant carrier proteins is responsible for efficient insertion into the inner mitochondrial membrane. J Mol Biol **351**: 16–25

Nolden M, Ehses S, Koppen M, Bernacchia A, Rugarli EI, Langer T (2005) The m-AAA protease defective in hereditary spastic paraplegia controls ribosome assembly in mitochondria. Cell **123**: 277–289

Opalinska M, Parys K, Murcha MW, Janska H (2018) The plant i-AAA protease controls the turnover of an essential mitochondrial protein import component. J Cell Sci **131**

Petereit J, Duncan O, Murcha MW, Fenske R, Cincu E, Cahn J, Pruzinska A, Ivanova A, Kollipara L, Wortelkamp S, et al. (2020) Mitochondrial CLPP2 assists coordination and homeostasis of respiratory complexes. Plant Physiol **184**: 148–164

Piechota J, Kolodziejczak M, Juszczak I, Sakamoto W, Janska H (2010) Identification and characterization of high molecular weight complexes formed by matrix AAA proteases and prohibitins in mitochondria of Arabidopsis thaliana. J Biol Chem **285**: 12512–12521

Quiros PM, Langer T, Lopez-Otin C (2015) New roles for mitochondrial proteases in health, ageing and disease. Nat Rev Mol Cell Biol **16**: 345–359

Schertl P, Braun HP (2015) Activity measurements of mitochondrial enzymes in native gels. Methods Mol Biol **1305**: 131–138

Schneider CA, Rasband WS, Eliceiri KW (2012) NIH Image to ImageJ: 25 years of image analysis. Nat Methods **9**: 671–675

Schreiner B, Westerburg H, Forne I, Imhof A, Neupert W, Mokranjac D (2012) Role of the AAA protease Yme1 in folding of proteins in the intermembrane space of mitochondria. Mol Biol Cell **23**: 4335–4346

Smakowska E, Skibior-Blaszczyk R, Czarna M, Kolodziejczak M, Kwasniak-Owczarek M, Parys K, Funk C, Janska H (2016) Lack of FTSH4 protease affects protein carbonylation, mitochondrial morphology, and phospholipid content in mitochondria of Arabidopsis: new insights into a complex interplay. Plant Physiol **171**: 2516–2535

Soufari H, Parrot C, Kuhn L, Waltz F, Hashem Y (2020) Specific features and assembly of the plant mitochondrial complex I revealed by cryo-EM. Nat Commun **11**: 5195

Steglich G, Neupert W, Langer T (1999) Prohibitins regulate membrane protein degradation by the m-AAA protease in mitochondria. Mol Cell Biol **19**: 3435–3442

Szczepanowska K, Senft K, Heidler J, Herholz M, Kukat A, Hohne MN, Hofsetz E, Becker C, Kaspar S, Giese H, et al. (2020) A salvage pathway maintains highly functional respiratory complex I. Nat Commun **11**: 1643

Tatsuta T, Augustin S, Nolden M, Friedrichs B, Langer T (2007) m-AAA protease-driven membrane dislocation allows intramembrane cleavage by rhomboid in mitochondria. EMBO J **26**: 325–335

Tatsuta T, Langer T (2009) AAA proteases in mitochondria: diverse functions of membrane-bound proteolytic machines. Res Microbiol **160**: 711–717

Urantowka A, Knorpp C, Olczak T, Kolodziejczak M, Janska H (2005) Plant mitochondria contain at least two i-AAA-like complexes. Plant Mol Biol **59**: 239–252

Vazquez-Calvo C, Suhm T, Buttner S, Ott M (2020) The basic machineries for mitochondrial protein quality control. Mitochondrion **50**: 121–131

Vierstra RD (2009) The ubiquitin-26S proteasome system at the nexus of plant biology. Nat Rev Mol Cell Biol **10**: 385–397

Voos W (2013) Chaperone-protease networks in mitochondrial protein homeostasis. Biochim Biophys Acta **1833**: 388–399

Wang Y, Carrie C, Giraud E, Elhafez D, Narsai R, Duncan O, Whelan J, Murcha MW (2012) Dual location of the mitochondrial preprotein transporters B14.7 and Tim23-2 in complex I and the TIM17:23 complex in Arabidopsis links mitochondrial activity and biogenesis. Plant Cell **24**: 2675–2695

Weigel D, Glazebrook J (2006) EMS mutagenesis of Arabidopsis seed. CSH Protoc **2006**

Westphal K, Langklotz S, Thomanek N, Narberhaus F (2012) A trapping approach reveals novel substrates and physiological functions of the essential protease FtsH in Escherichia coli. J Biol Chem **287**: 42962–42971

Zhang S, Li C, Wang R, Chen Y, Shu S, Huang R, Zhang D, Li J, Xiao S, Yao N, et al. (2017) The Arabidopsis mitochondrial protease FtSH4 is involved in leaf senescence via regulation of WRKY-dependent salicylic acid accumulation and signaling. Plant Physiol **173**: 2294–2307

Zhang S, Wu J, Yuan D, Zhang D, Huang Z, Xiao L, Yang C (2014a) Perturbation of auxin homeostasis caused by mitochondrial FtSH4 gene-mediated peroxidase accumulation regulates Arabidopsis architecture. Mol Plant **7**: 856–873

Zhang S, Zhang D, Yang C (2014b) AtFtsH4 perturbs the mitochondrial respiratory chain complexes and auxin homeostasis in Arabidopsis. Plant Signal Behav **9**: e29709

Zurita Rendon O, Shoubridge EA (2012) Early complex I assembly defects result in rapid turnover of the ND1 subunit. Hum Mol Genet **21**: 3815–3824